Korean J. Chem. Eng., 40(4), 925-934 (2023)
DOI: 10.1007/s11814-022-1303-0

pISSN: 0256-1115
eISSN: 1975-7220

Separation of CO_2 and H_2S from natural gas of iranian gas refinery using ionic liquids: Experimental measurements and thermodynamic modeling

Ramesh Rezaeinejad*, Amir Abdolah Mehrdad Sharif*,†, and Fariborz Shaahmadi**

*Department of Analytical Chemistry, Faculty of Chemistry, Islamic Azad University, North Tehran Branch, Tehran, Iran
**Department of Process Engineering, Stellenbosch University, Banghoek Road, Stellenbosch, 7600, South Africa
(*Received 7 May 2022 • Revised 23 September 2022 • Accepted 25 September 2022*)

Abstract−Separation of the acid gases and reducing their amount from natural gas is very important in the gas purification industries. In this study, the solubility of natural gas (a mixture of CO_2, H_2S, CH_4, C_2H_6, etc.) was experimentally measured in three different ionic liquids: 1-hexyl-3-methylimidazolium bis(trifluoromethylsulfonyl) imide ([Hmim][Tf_2N]), 1-hexyl-3-methylimidazolium nitrate ([Hmim][NO_3]) and 1-butyl-3-methylimidazolium acetate ([Bmim][Ac]). The experimental solubility data was obtained for the temperatures of 298.15 K, 318.15 K, and 338.15 K in pressure range up to 40 bar. Selectivity of CO_2/CH_4, CO_2/H_2S and H_2S/CH_4 in the studied ionic liquids was also reported in this work. [Bmim][Ac] showed the best performance of absorbing CO_2 and H_2S compared to other ionic liquids. However, [Hmim][Tf_2N] showed higher selectivity for CO_2 over CH_4 in comparison with [Hmim][NO_3] and [Bmim][Ac]. Finally, the sPC-SAFT equation of state was successfully used to predict the natural gas solubility in ionic liquids. The results show that the model predictions are consistent with experimental data.

Keywords: CO_2, H_2S, Ionic Liquids, Natural Gas, sPC-SAFT

INTRODUCTION

A typical gas treating process involves the reduction of the acid gas content (CO_2, H_2S), along with other sulfur species, to a specific level to meet the standards or allow additional processing in the gas plant without corrosion or other known problems. Acidic gases, including CO_2 and H_2S, can lead to severe problems, such as toxicity, equipment corrosion, the low heating value of natural gas, and hydrate formation during natural gas liquefaction process [1,2]. Alkanolamines are the main commercial solvents widely used for CO_2 and H_2S removal in natural gas processing due to their high absorption capacity. However, these solvents have several serious problems, such as solvent degradation, high volatility, low selectivity toward CO_2/H_2S, corrosivity and high energy demand for their regeneration [3-5]. In the last two decades, a new kind of solvent has gained notable consideration, known as ionic liquids (ILs). IL with an organic cation and organic or inorganic anion, which is in the molten salt state under 100 °C, is called room temperature ionic liquid (RTILs). The various cations and anions can be used to synthesize an IL with specific properties. Appropriate cations and anions are required to obtain RTIL solvents with specific physical, chemical, or biological characteristics. Due to negligible vapor pressure, the ILs are considered nonvolatile materials with environmentally friendly behavior [6-10]. ILs can be distinguished from conventional solvents by their characteristic properties and have emerged as a new class of solvents called "green solvents" in different engineering applications. Among various applications of ILs, they have been used for CO_2 and H_2S capture and they have shown great potential to overcome many challenges in current technologies associated with CO_2 and H_2S capture [11-13]. Considering different methods suggested in the literature, ILs have shown great potential to overcome these problems due to their negligible volatility, high thermal stability and non-corrosivity. They can be superior to the classical solvents due to these characteristic properties [14-18].

Many ILs are introduced and employed for CO_2 capture in the literature [16]. Baltus et al. [16] employed imidazolium based ILs at low CO_2 partial pressure. They concluded that increasing the length of alky chain on the imidazolium ring increased the solubility of CO_2. Experimental and molecular dynamic simulation of CO_2 solubility in ILs are investigated by Cadena et al. [17]. They found that the nature of the anion had the dominant effect on the solubility of CO_2. According to their results, ILs with $[Tf_2N]^-$ ions had the highest affinity towards CO_2. Aki et al. [18] also investigated ILs with different anions and with the same cation. The solubility of CO_2 was increased by increasing the fluorine atoms in anions. This result contributed to the strong coulombic infractions that are responsible for liquid organizations and it was proved by Kumar et al. [11] as well. Kumar et al. [11] showed that the ILs with Tf_2N−anions had higher solubility for CO_2 compared to ILs with PF_6−anions, which confirms the other researches. Many solubility data on ILs, have been reported in literature [19], but there is very little data on the selectivity of CO_2 with other gases, including CH_4 ,C_2H_6, H_2S. However, the solubility and selectivity of CO_2 over different hydrocarbons species in the real natural gas are scarce [20]. On the other hand, literature regarding the H_2S solubility on ILs is also limited to a few investigations [21].

According to the work conducted on gas solubility in ILs, it was found that increasing pressure has a positive effect on H_2S and CO_2

†To whom correspondence should be addressed.
E-mail: a_sharif@mail.iau-tnb.ac.ir

Table 1. The detailed of materials and gas mixture used in this study

Chemical name	Chemical formula	CAS No.	Company	Purity	Molecular weight	Purification method
1-Hexyl-3-methylimidazolium bis(trifluormethylsulfonyl)imide [Hmim][Tf_2N]	$C_{12}H_{19}F_6N_3O_4S_2$	382150-50-7	Sigma-Aldrich 727954	≥98% (HPLC)	447.42	Supplier data
1-Butyl-3-methylimidazolium acetate [Bmim][Ac]	$C_{10}H_{18}N_2O_2$	284049-75-8	Sigma-Aldrich 30367	≥96.0% HPLC	198.26	Supplier data
1-Hexyl-3-methylimidazolium Nitrate [Hmim][NO_3]	$C_{10}H_{19}N_3O_3$	203389-26-8	Atlas Shimi Sabz	≥96.0% HPLC	229.28	Supplier data
Natural gas cylinder (120 bar)	-	-	Bidboland Gas refinery	GC analyzed	-	Analyzed by GC

solubility, while increasing temperature showed an adverse effect of solubility. Also, it was found that solubility of H_2S in pure state is higher than that of CO_2 [22]. However, there is no reported data for the selectivity of these gases on ILs from real mixed gas feed. In addition, H_2S is more soluble in [Emim][Tf_2N] IL, and it was concluded that as for CO_2, the anion part had more profound effect on H_2S solubility in imidazolium based ILs. It was revealed that in a [Hoemim] based ILs, H_2S is more soluble than CO_2; but with increasing the trifluoro methyl (CF_3) groups in the anions, the solubility increased for both H_2S and CO_2 [21,23,24]. The aforementioned investigation found that H_2S solubility in ILs is physical and the imidazolium based ILs are the most common ILs employed for CO_2 and H_2S capture [25,26].

Numerous studies have been conducted for pure CO_2 (or H_2S) solubility in ILs, but very few literature data are available for selectivity of CO_2/CH_4, H_2S/CH_4 and CO_2/H_2S. In addition, the available data for CO_2 and H_2S capture from real natural gas is very scant, to our knowledge. On the other hand, application of ILs in industrial applications requires the behavior of ILs for CO_2 and H_2S capture from the real gas. This work aimed to investigate the solubility of CH_4, H_2S and CO_2 from a real gas sample, in the three ILs [Hmim][Tf_2N], [Hmim][NO_3], and [Bmim][Ac] at temperatures of 298.15 K, 318.15 K and 338.15 K and pressures up to 40 bar. The capability of these ILs was investigated in terms of solubility and selectivity for CH_4, CO_2, and H_2S in the gas sweetening process. Furthermore, sPC-SAFT EoS was applied to model the measured solubility of the natural gas in studied ILs.

MATERIAL AND METHODS

1. Materials

The ILs used in present study were: 1-Hexyl-3-methylimidazolium bis(trifluormethylsulfonyl)imide ([Hmim][Tf_2N]) and 1-butyl-3-methylimidazolium acetate ([Bmim][Ac]) were purchased from Sigma Aldrich; and 1-Hexyl-3-methylimidazolium Nitrate ([Hmim][NO_3]) was purchased from Atlas shimi Sabz Co. (Iran). Due to the impact of water and volatile compound's presence on the performance of the ionic liquids, it is necessary to reduce these compound's concentration to an acceptable level, to ensure that they cannot affect the IL performance during the process. Therefore, in this study, the ILs were degassed and dried with stirring at high temperature (70 °C for 20 h) under vacuum. Then, the water content of ILs was measured by a Mettler Toledo DL38 Karl Fischer Titrator. The natural gas used in this study was a real natural gas mixture provided by Bidboland (Khozestan, Iran) gas refinery. The gas mixture was analyzed by three different gas chromatograph systems, and the concentration varied within the ±0.1 mol% for three measurements. The gas mixture included (mol%) methane (86.59%), ethane (5.83%), propane (2.57%), i-butane (0.45%), n-butane (0.81%), i-pentane (0.31%), n-pentane (0.32%), i-hexane (0.18%), n-hexane (0.12%), i-heptane (0.036%), n-heptane (0.03%), H_2S (0.025%), N_2 (0.21%) and CO_2 (2.52%). The details of all utilized chemicals and gas mixture are presented in Table 1 and Fig. 1.

2. Experimental Apparatus and Procedure

The apparatus, built in-house by Shaahmadi et al. [27], was used for measuring the gas solubility in ILs as schematically shown in Fig. 2. This apparatus includes two pressure transmitter sensors (Ps1 and Ps2), a temperature sensor, (Ts) and six ball valves (V_1-V_3, V_5-V_7), a needle valve (V_4) and a micro valve (V_8), a high-pressure stainless-steel cell, a circulator with temperature control system, and a data acquisition device connected to a computer. The V_4 was used for connecting the system to a vacuum pump. The circulator was used to maintain equilibrium cell temperature at desired value. Ps1 sensor read the gas pressure prior to injection and Ps2 measured the equilibrium cell pressure. In a typical test, a known mass of ILs was placed into the equilibrium cell, and then the entire system was evacuated by a vacuum pump through V_4.

The cell temperature was set to the desired value by a circulator. Afterwards, V_5 was opened, and a known amount of gas was introduced into the equilibrium cell (volume of each section of the set-up is known). The amount of gas injected into the cell was calculated by Eq. (1).

$$n_{gas} = \frac{V}{RT}\left(\frac{P_i}{Z_i} - \frac{P_f}{Z_f}\right) \quad (1)$$

where V is volume of the bomb, T is the temperature of the gas and

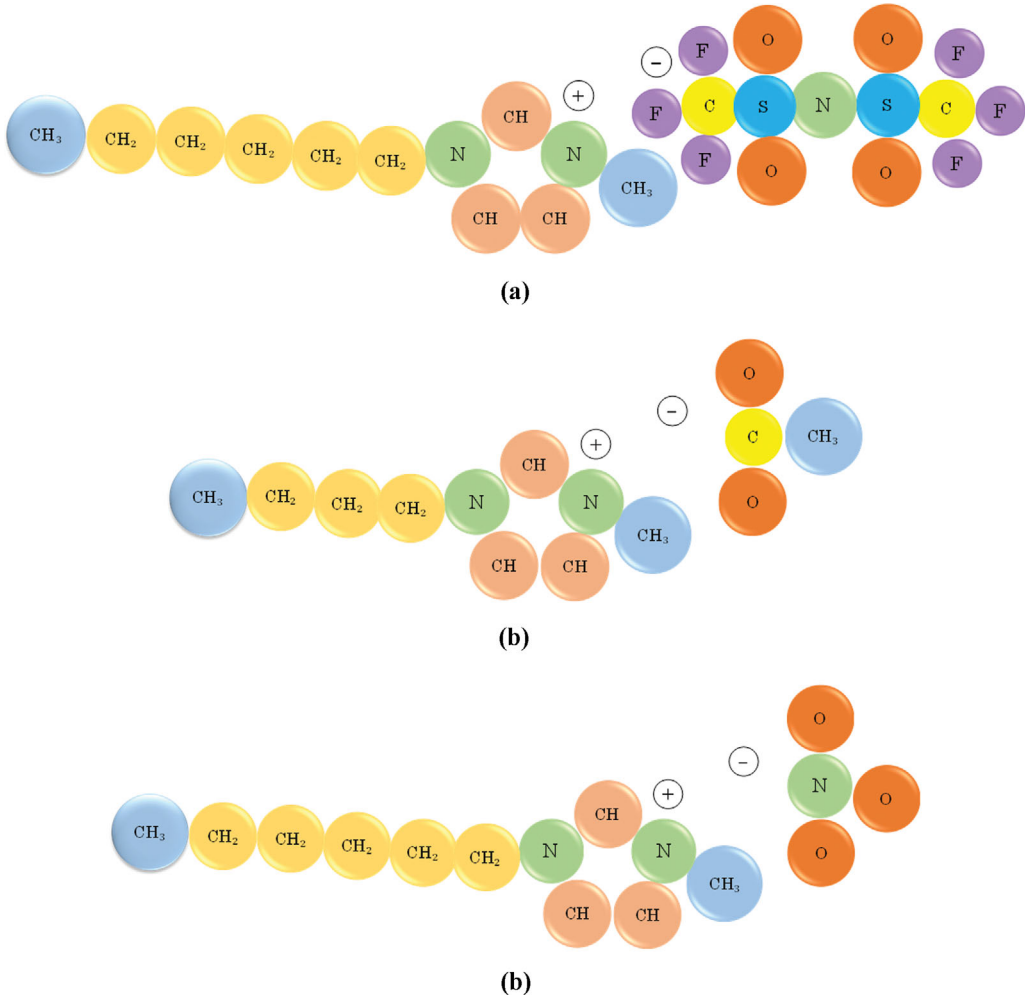

Fig. 1. The structure of ILs studied in this work: (a) [Hmim][Tf_2N]; (b) [Bmim][Ac]; and (c) [Hmim][NO_3].

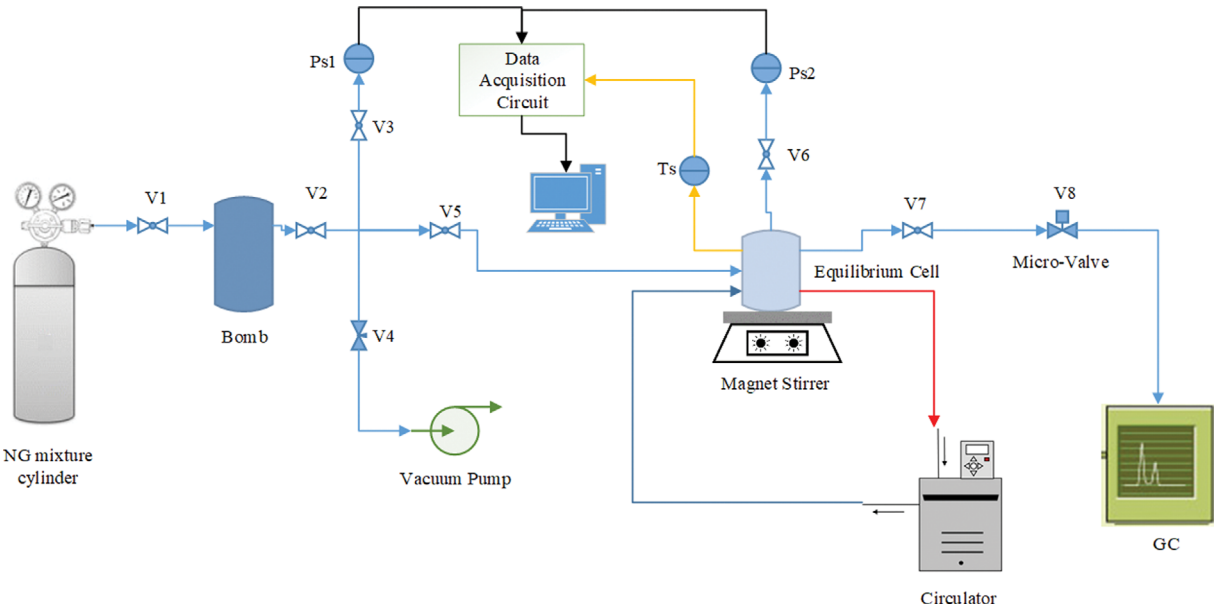

Fig. 2. Experimental apparatus for measuring gas solubility in IL used in this work (re-drawn and adapted with permission from Shaahmadi et al. [27]).

R is the universal gas constant. P_i and P_f are the initial and final pressures obtained from the Ps1 sensor. Z_i and Z_f are the compressibility factors for the initial and final pressures and temperature of the bomb, respectively. sPC-SAFT EoS was used to calculate the compressibility factors in vapor phase. After contacting IL with natural gas, equilibrium was achieved when the pressure change in the system became constant over time (P_{equil}). The moles of components (natural gas components) remaining in the gas phase ($n_{g,gas}$) can be obtained by using an appropriate equation of state at P_{equil}, T of the cell, and volume of the system from V_5 to cell. The moles of components in the liquid phase $n_{l,gas}$ were determined by Eq. (2).

$$n_{l,gas}=n_{gas}-n_{g,gas} \tag{2}$$

The gas chromatograph (GC) was used for the gas analysis of the gas phase ($n_{g,gas}$) to quantify the mole fraction of each component in the gas phase. Agilent 7098 GC was equipped with an FPD detector for analysis of H_2S, and a TCD detector for analysis of CO_2, and an FID detector for hydrocarbon concentration measurement. The GC column for FPD was Silica PLOT capillary column 30 m× 0.32 mm, film thickness 4 μm. The channel of FPD detector on GC for H_2S measurement was calibrated for two ranges of low level and high level. Finally, the solubility of each component (CO_2, H_2S, CH_4, etc.) was obtained by mass balance for each of them.

3. Thermodynamic Modeling

A simplified perturbed chain-statistical associating fluid theory (sPC-SAFT) equation of state (EoS) was developed with the idea of reducing the computational effort of the PC-SAFT model without disturbing the model performance. The sPC-SAFT in the case of single non-associating compounds is identical to the PC-SAFT, but when multicomponent mixtures are involved, they are not the same. In practice, the sPC-SAFT uses a simpler mixing rule where it assumes that the segment diameters belonging to different molecules are usually the same [28]. sPC-SAFT EoS uses simplified expressions for the hard-chain term ($\tilde{a}^{hc}$) and the radial distribution function in association term ($\tilde{a}^{assoc}$).

The Helmholtz energy of a mixture with associating molecules is described by Eq. (3).

$$\tilde{a}=\frac{A}{nkT}=\tilde{a}^{id}+\tilde{a}^{hc}+\tilde{a}^{disp}+\tilde{a}^{assoc} \tag{3}$$

where $\tilde{a}^{id}$ represents the ideal gas contribution, $\tilde{a}^{hc}$ is the hard-sphere chain, $\tilde{a}^{disp}$ is the contribution of dispersion forces and finally, the $\tilde{a}^{assoc}$ accounts for the contribution of association. In the sPC-SAFT, the ideal gas contribution and dispersion are the same as the original PC-SAFT. The difference is in the hard-chain and association forces. According to sPC-SAFT as mentioned above, we assumed a single diameter for all segments. This diameter is calculated according to Eq. (4) [28],

$$d_{av}^{n}=\left(\frac{\Sigma_i x_i m_i d_i^3}{\Sigma_i x_i m_i}\right)^{1/3} \tag{4}$$

and ξ_n calculated by Eq. (5):

$$\xi_n=d_{av}^{n}\frac{\pi}{6}\rho\Sigma_i x_i m_i \tag{5}$$

The setting $\eta=\xi_3$, the following expression for g^{hs} and $\tilde{a}^{hc}$, was derived (Eqs. (5) and (6)) [28].

$$g^{hs}=\frac{1-\frac{\eta}{2}}{(1-\eta)^3} \tag{6}$$

$$\tilde{a}_{CS}^{hc}=\frac{4\eta-3\eta^2}{(1-\eta)^2} \tag{7}$$

g^{hs} is applied in $\tilde{a}^{assoc}$ term of Helmholtz free energy as follows:

$$\tilde{a}^{assoc}=\Sigma_{i=1}^{n_c}x_i\left[\Sigma_{A_i}\left(\ln X^{A_i}-\frac{X^{A_i}}{2}\right)+\frac{1}{2}M_i\right] \tag{8}$$

where X^{A_i} is the mole fraction of molecules i not bonded at site A, M_i is the number of association sites on each molecule, and Σ_{A_i} represents a sum over all associated sites on each molecule. The parameter X^{A_i} is defined as

$$X^{A_i}=[1+N_{Av}\Sigma_j\Sigma_{B_j}\rho_j X^{B_i}\Delta^{A_iB_j}]^{-1} \tag{9}$$

The association strength $\Delta^{A_iB_j}$ for sPC-SAFT EoS is given by

$$\Delta^{A_iB_j}=g_{ij}^{hs}\left[\exp\left(\frac{\varepsilon^{A_iB_j}}{kT}\right)-1\right](\sigma_{ij}^3\kappa^{A_iB_j}) \tag{10}$$

The interaction parameter for sPC-SAFT is the same as the original PC-SAFT by Eq. (11).

$$\varepsilon_{ij}=\sqrt{\varepsilon_i\varepsilon_j}(1-k_{ij}) \tag{11}$$

where k_{ij} is the binary interaction parameter between species in the mixture. k_{ij} can be adjusted using vapor-liquid equilibrium (VLE) properties of the mixture. In this study, binary interaction parameters were not considered to investigate the predictivity of sPC-SAFT EoS (k_{ij}=0).

And as for σ_{ij}, the conventional combining rule is applied by Eq. (12).

$$\sigma_{ij}=\frac{\sigma_i+\sigma_j}{2} \tag{12}$$

The reader is referred to the original sPC-SAFT for the details of the model [28].

3-1. Model Parameters

The sPC-SAFT EoS's parameters for pure ILs were adjusted from the available experimental density data in the literature. Note that vapor pressure data for the studied ILs is scarce and excluded from optimization procedure. The sPC-SAFT parameters for the natural gas components were obtained from the literature. The whole set of the parameters is presented in Table 2. According to available literature data for studied ILs, only one set of data was considered for obtaining EoS's parameters through an optimization procedure. Then, sPC-SAFT EoS was applied to predict the density of ILs for other literature data. The details of average absolute relative deviation (AARD) of density for the studied ILs are reported in Table 3. The results show that sPC-SAFT EoS can successfully predict the density of ILs with very low values of AARD%.

RESULT AND DISCUSSION

Solubility is one of the important parameters in vapor liquid equi-

Table 2. Pure compound parameters for sPC-SAFT EoS

Compound	M (g/mol)	T-range (K)	m (-)	σ (Å)	ε/k (K)	κ^{AB} (-)	ε^{AB}/k (K)	AAD%		Reference
								P	ρ	
[bmim][Ac]	198.27	298-353	3.092836	4.6887	691.16	0.02	3450	-	0.07	This work
[hmim][NO_3]	229.28	293-363	2.702808	4.9654	547.50	0.02	3450	-	0.06	This work
[hmim][Tf_2N]	447.41	293-338	11.4032	3.5043	306.67	0.02	3450	-	0.21	This work
CO_2	44.01	216-304	2.0729	2.7852	169.21	-	-	2.78	2.73	[29]
N_2	28.01	63-126	1.2053	3.3130	90.96	-	-	0.34	1.5	[29]
H_2S	34.08	187-336	1.6800	3.0250	26.70	-	-	0.14	0.43	[30]
CH_4	16.043	97-300	1.0000	3.7039	150.03	-	-	0.36	0.67	[29]
C_2H_6	30.07	90-305	1.6069	3.5206	191.42	-	-	0.3	0.57	[29]
C_3H_8	44.096	85-523	2.0020	3.6184	208.11	-	-	1.29	0.77	[29]
iC_4	58.123	113-407	2.2616	3.7574	216.53	-	-	0.55	1.47	[29]
nC_4	58.123	135-573	2.3316	3.7086	222.88	-	-	0.75	1.59	[29]
iC_5	72.15	113-460	2.5620	3.8296	230.75	-	-	0.4	1.53	[29]
nC_5	72.146	143-469	2.6896	3.7729	231.2	-	-	1.45	0.78	[29]
iC_6	86.177	119-498	2.9317	3.8535	235.58	-	-	0.61	0.59	[29]
nC_6	86.177	177-503	3.0576	3.7983	236.77	-	-	0.31	0.76	[29]
iC_7	100.204	154-530	3.3478	3.8612	237.42	-	-	0.74	1.44	[29]
nC_7	100.203	182-623	3.4831	3.8049	238.4	-	-	0.34	2.1	[29]

Table 3. The average absolute relative deviations (%AARD) of density for studied ionic liquids

Component	T range (K)	P range (bar)	N_p	%AARD (ρ)	Ref.
[Hmim][Tf_2N]	273.13-413.17	1.01-1400	266	0.45**	[31]
	312.6-452.3	1-2000	168	0.53**	[32]
	293.15-338.15	1-650.2	163	0.21*	[33]
	298.15-333.15	1-595.9	156	0.14**	[34]
	273.15-363.15	1.01325	39	0.27**	[35]
[Hmim][NO_3]	293.15-363.15	1.01325	8	0.06*	[36]
	293.15-323.15	1.01325	7	0.08**	[37]
[Bmim][Ac]	311.4-371.3	100-2000	80	1.46**	[38]
	298.09-353.08	1-250	63	0.07*	[39]
	283.15-363.15	1.01325	17	0.12**	[40]
Total			967		

* Included in parameter regression.

** Not included in parameter regression.

libria when investigating CO_2 and H_2S loading of solvent in the absorption process. CO_2 and H_2S solubility of pure ILs is an important parameter when one wants to evaluate the hybrid solvents as well. The in-house apparatus (Fig. 1) was successfully used in previous work for gas solubilities in ILs [20,27]. The experiments on solubility measurement of real natural gas compounds in three ILs, including [Hmim][Tf_2N], [Hmim][NO_3] and [Bmim][Ac], were conducted at 298.15 K, 318.15 K, and 338.15 K for the pressure range up to 40 bar. The temperature and pressure range was selected based on the industrial practices. Uncertainty values for temperature, pressure and solubility were ±0.2 K, ±0.002 bar, and ±0.0001, respectively. The solubility of gases in ILs is presented as mole fraction of the gas in liquid phase (such as x_{CO_2}).

Fig. 3 shows the results of CH_4, CO_2 and H_2S solubility in studied ILs at 298.15 K. Although, the mole fraction of CH_4 is higher in feed (86.59%) compared to CO_2 (2.52%). To better compare the studied ILs for gas solubility of natural gas, the following figures are presented to show the solubility of each gas (CO_2, H_2S, and CH_4) separately.

Fig. 4 depicts the CO_2 solubility in three different pure ILs at 298.15 K, 318.15 K, and 338.15 K. The CO_2 solubility at different temperatures for studied ILs is presented in the figure as well to compare the capability of the solvents. According to Fig. 4, the solubility of CO_2 in [Bmim][Ac] was higher than that of [Hmim][Tf_2N] and [Hmim][NO_3]. Many studies have shown that the effect of anion part interaction with CO_2 in ILs has a much stronger effect on the solubility of CO_2 [10,17]. Another important parameter that affects the solubility of CO_2 in ILs is their relative size in sys-

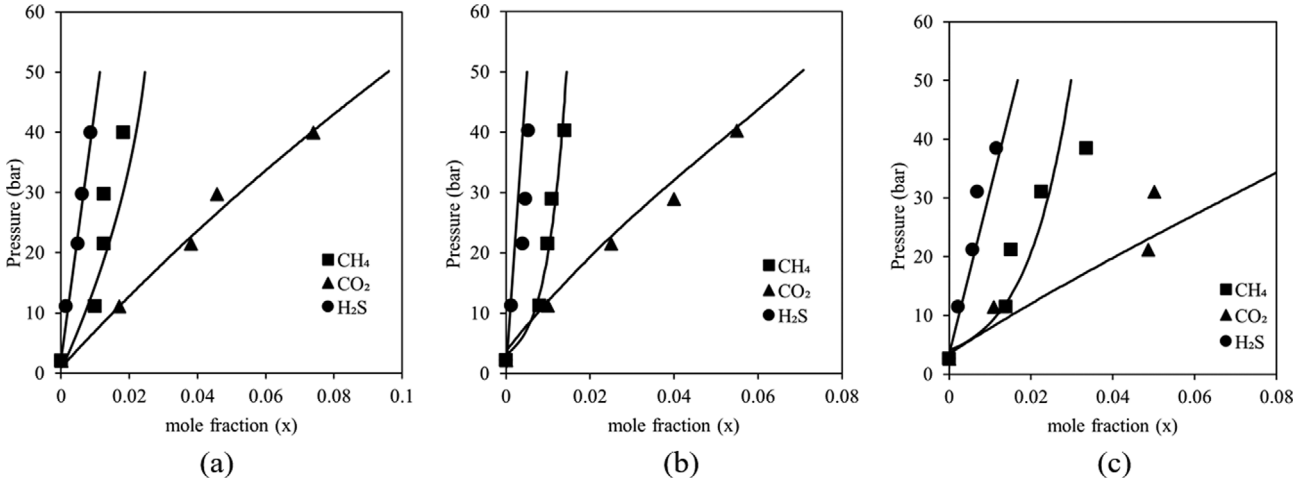

Fig. 3. The comparison of CH_4, CO_2 and H_2S solubility in studied ILs at T=298.15 K: (a) [Hmim][Tf_2N]; (b) [Hmim][NO_3]; and (c) [Bmim][Ac]. Continuous curves are sPC-SAFT EoS prediction results.

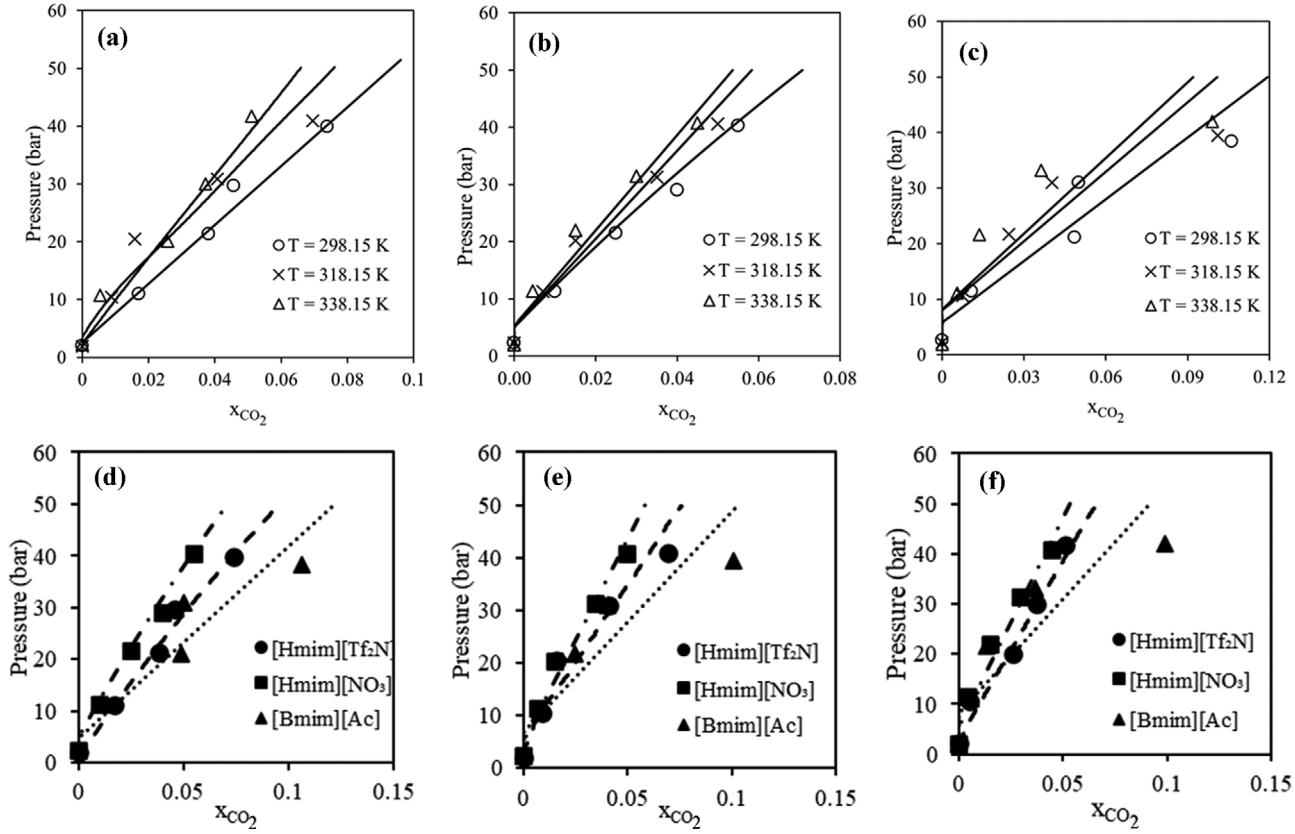

Fig. 4. CO_2 solubility data for (a) [Hmim][Tf_2N], (b) [Hmim][NO_3], (c) [Bmim][Ac], (d) IL's comparison at 298.15 K, (e) IL's comparison at 318.15 K and (f) IL's comparison at 338.15 K. Continuous curves are sPC-SAFT EoS prediction results (k_{ij}=0).

tems that involve the physisorption process, while the interaction of solvent-solute plays a minor role in the solubility. As for systems that involve chemisorption, the interaction of solute and the solvent is the main reason for solubility. In such systems, the type of interaction between solute-solvent has a dominant effect on the solubility. It was shown that the solubility of CO_2 in [Bmim][Ac] is of chemisorption type. Therefore, in CO_2/[Bmim][Ac] system, the polar interactions are much stronger and are responsible for higher CO_2 solubility compared to two other ILs. On the other hand, the anionic effect of [Tf_2N] is stronger than [NO_3], because the presence of fluoroalkyl substituents has a more favorable interaction with CO_2. As temperature increased, the amount of solubility of CO_2 for all ILs reduced. It can be seen that increasing temperature has less effect on solubility of [Bmim][Ac], but its effect on solubil-

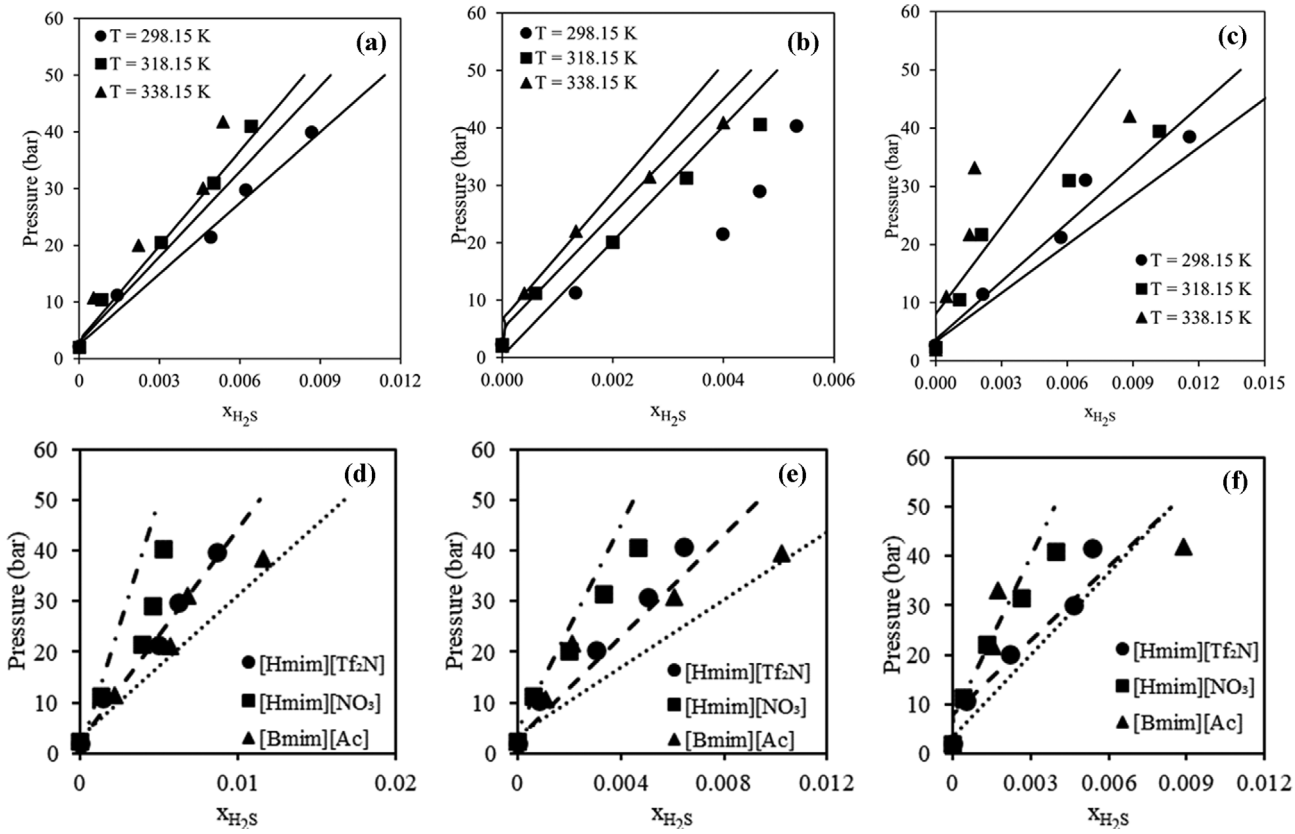

Fig. 5. H_2S solubility data for (a) [Hmim][Tf_2N], (b) [Hmim][NO_3], (c) [Bmim][Ac], (d) IL's comparison at 298.15 K, (e) IL's comparison at 318.15 K and (f) IL's comparison at 338.15 K. Continuous curves are sPC-SAFT EoS prediction results (k_{ij}=0).

ity reduction of [Hmim][Tf_2N] is more noticeable than [Hmim][NO_3]. It can be explained by the fact that chemisorption of [Bmim][Ac] is less affected by increasing temperature than physical interactions responsible for the physisorption of CO_2 in other two ILs.

As can be seen, a maximum mole fraction of about 0.11 CO_2 for [Bmim][Ac] was obtained at 298.15 K and total pressure of near 40 bar. The solubility data reported in this work is lower than that of other related literatures. The reason is that a real natural gas was used in this work in which the CO_2 concentration was about 2.52 mole percent. While in other literatures mostly pure CO_2 gas was used. Solubility from a gas mixture where the partial pressure of solute is low, not comparable to that of solute pure gas phase.

The H_2S solubility data from real natural gas into the studied ILs presented in Fig. 5. As shown in Fig. 5, the solubility of H_2S decreased by increasing temperature for all three ILs and increased by increasing pressure as expected. Comparison of the solubility of three ILs at different temperatures shows that the [Hmim]NO_3] has lower solubility than [Hmim][Tf_2N] and [Bmim][Ac]. The reduction in solubility of H_2S with increased temperature is less pronounced for [Bmim][Ac]. But its effect on [Hmim][Tf_2N] is more distinct than [Hmim][NO_3]. The reason for lower solubility of H_2S in [Hmim][NO_3] can be attributed to the lower electronegativity of anion part of IL.

As for other two ILs, the free electrons on the [Tf_2N] and [Ac] can interact with H_2S molecules. Therefore, increasing its solubility in corresponding ILs. The higher value of solubility for [Bmim][Ac] can be attributed to the chemisorption nature of this system. In addition, this can be the main reason why the effect of increasing temperature was less pronounced on solubility of this IL. In literature, it was stated that solubility of H_2S is more energetic than CO_2 in ILs [41]. However, in this work, small values of H_2S solubility into the ILs were reported due to very small concentration of H_2S in the real natural gas mixture that was used in this study. The initial concentration of H_2S in gas feed mixture was 251 ppm. Despite very low concentration, its solubility in [Bmim][Ac] is nearly 0.009 mole fraction at temperature of 298.15 K and pressure of 40 bar. The interaction of H_2S with [Tf_2N] anion is stronger than its interaction with CO_2. If the concentration of both species was at the same order of magnitude, it was expected to observe a higher solubility value for H_2S than CO_2 on [Hmim][Tf_2N]. However, due to very much lower concentration (about two orders of magnitude less than CO_2), its solubility is about one order of magnitude lower than CO_2.

The solubility of all hydrocarbons presented in real natural gas measured and the results were presented in supporting information (ST-1). However, for methane the solubility data are shown in Fig. 6.

As can be seen from the results shown in Fig. 6, the solubility of CH_4 is decreased by increasing temperature from 298.15 K to 338.15 K and increased by increasing pressure as observed for both CO_2 and H_2S. Comparing the solubility of different ILs at different temperatures shows that the solubility of methane in [Bmim][Ac]

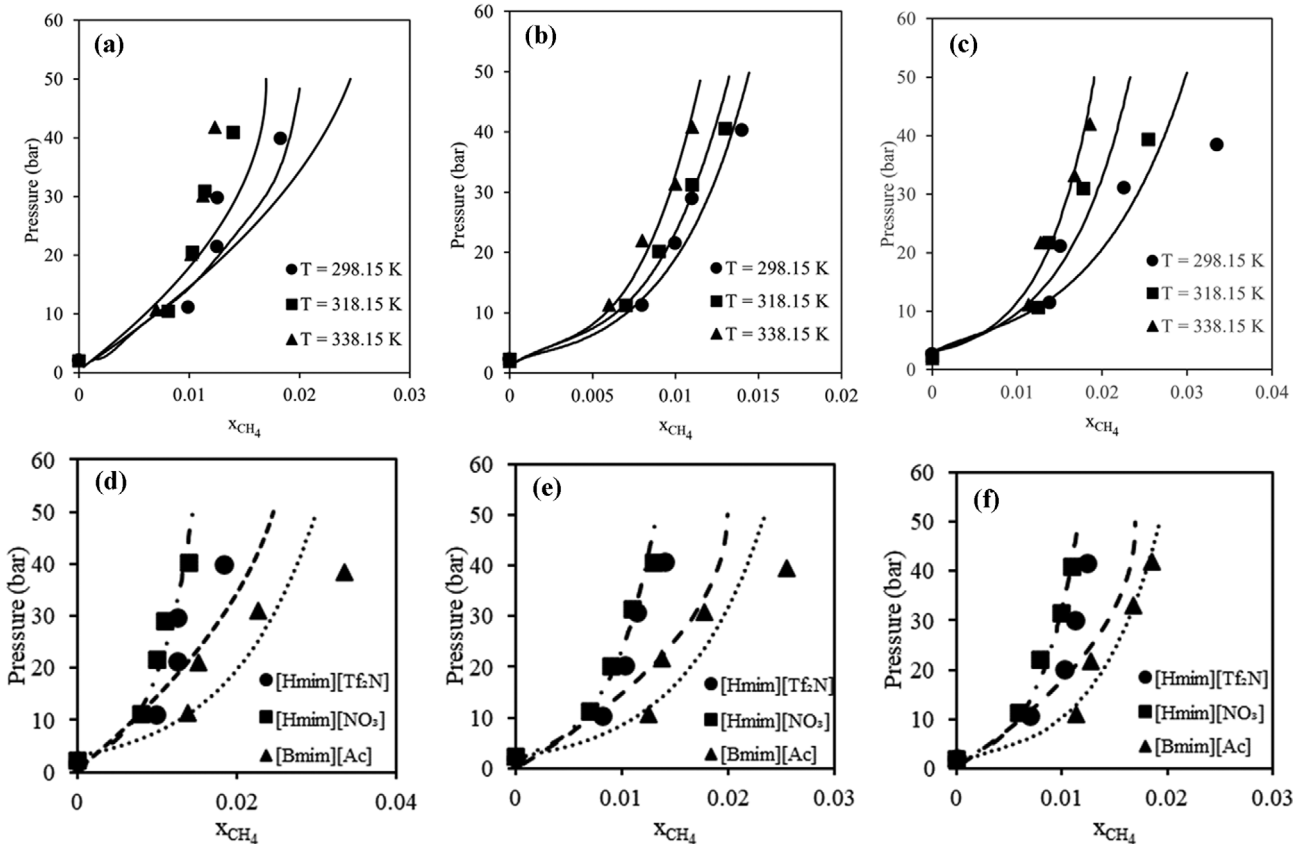

Fig. 6. CH_4 solubility data for (a) [Hmim][Tf_2N], (b) [Hmim][NO_3], (c) [Bmim][Ac], (d) ILs comparison at 298.15 K, (e) ILs comparison at 318.15 K and (f) ILs comparison at 338.15 K. Continuous curves are sPC-SAFT EoS prediction results (k_{ij}=0).

is much higher than that of [Hmim][NO_3] and [Hmim][Tf_2N]. On the other hand, the effect of temperature on the solubility reduction of methane for [Bmim][Ac] is more pronounced than the other two ILs. It was shown that the longer alkyl chain in ions of IL can increase the solubility of hydrocarbons. In [Bmim][Ac], the anion part has one alkyl group, while in [Hmim][Tf_2N] and [Hmim][NO_3], the anion part has no alkyl group. It can be argued that the cation part of [Hmim][Tf_2N] and [Hmim][NO_3] has a longer alkyl chain and should have shown higher solubility, but the results of this work did not confirm that. Based on these results, it can be concluded that the anion part of ILs plays a stronger role in solubility.

In contrast to solubility data of real gas components including CH_4, CO_2 and H_2S, it can be seen that [Bmim][Ac] has higher solubility toward CO_2 considering its mole fraction in real natural gas sample used in this study. As for H_2S, considering its low initial concentration in the gas phase, its solubility in all three ILs was high. By comparing these three ILs, it can be concluded that [Bmim][Ac] has higher solubility toward different components in real natural gas. The high solubility for desired species is a good characteristic for a solvent. But the selectivity is the key parameter in selecting a candidate solvent for the acid gas absorption process. The separation performance of the absorption process could be evaluated by measuring the selectivity of CO_2 (or H_2S) toward CH_4 (and other hydrocarbons). In this work, based on experimental solubility data, the selectivity of the H_2S, CO_2 and CH_4 was calculated by Eq. (13).

$$\text{Selectivity}_{i/j}=\frac{y_i/x_i}{y_j/x_j} \tag{13}$$

where i and j denote CO_2, H_2S and CH_4 and y_i and x_i are the vapor and liquid phase composition of gases obtained from VLE for at a constant temperature and pressure.

The CO_2/CH_4 selectivity for three ILs at different temperature is presented in Fig. 8.

As it can be seen, the selectivity value based on experimental data shows that by increasing pressure the selectivity of CO_2 to CH_4 increased for all ILs. Also, the increasing temperature did not show a clear trend for [Hmim][Tf_2N] and [Bmim][Ac]. Although, its trend is decreasing for [Hmim][NO_3] but is not significant. Another noteworthy point in Fig. 7 is that the [Hmim][Tf_2N] has a higher selectivity for CO_2 over methane in comparison to [Hmim][NO_3] and [Bmim][Ac]. Despite the higher CO_2 solubility of [Bmim][Ac], its selectivity over methane is lower than that of the other two ILs.

The H_2S/CH_4 selectivity of ILs is calculated and illustrated in Fig. 8.

As results are shown in Fig. 8, the selectivity of H_2S/CH_4 does not show a clear trend for [Hmim][Tf_2N], except that by increasing pressure the selectivity of H_2S over methane increased. The same

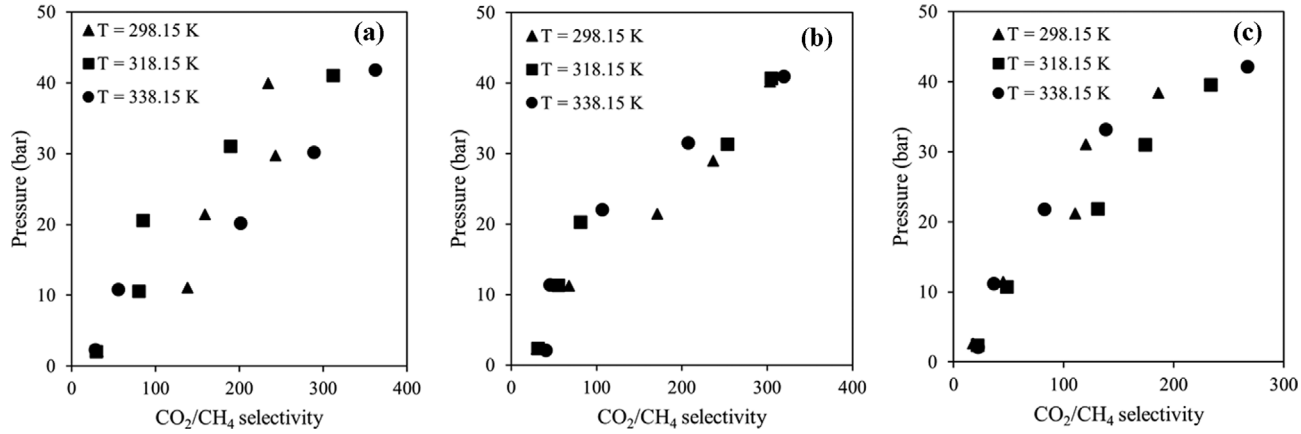

Fig. 7. The CO_2/CH_4 selectivity of three ILs: (a) [Hmim][Tf_2N]; (b) [Hmim][NO_3]; and (c) [Bmim][Ac].

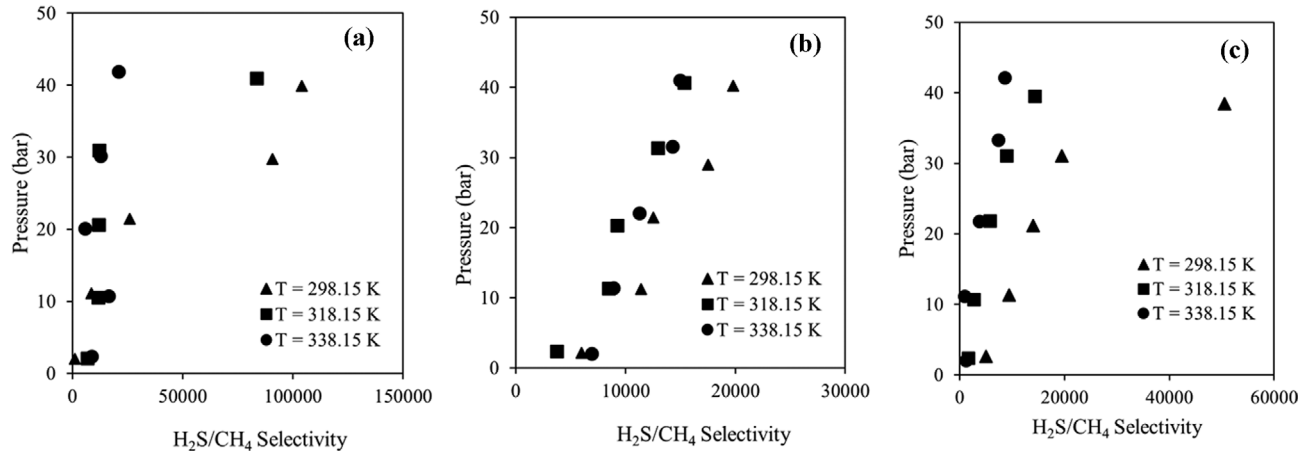

Fig. 8. H_2S/CH_4 selectivity for three ILs: (a) [Hmim][Tf_2N]; (b) [Hmim][NO_3]; and (c) [Bmim][Ac].

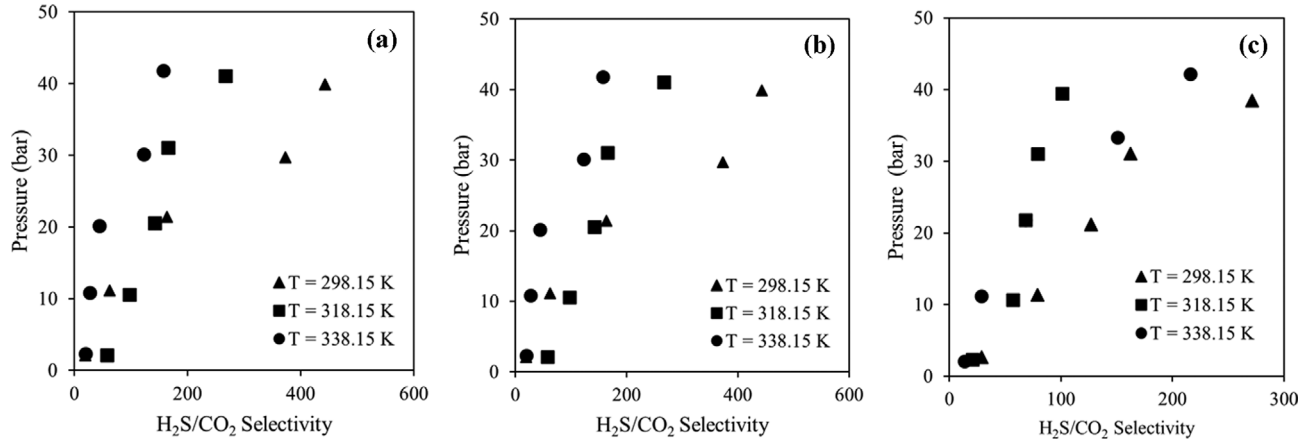

Fig. 9. H_2S/CO_2 selectivity of three ILs: (a) [Hmim][Tf_2N]; (b) [Hmim][NO_3]; and (c) [Bmim][Ac].

trends were observed for the other two ILs. Increasing temperature reduced the selectivity of H_2S over CH_4 for [Bmim][Ac]. As for [Hmim][NO_3], increasing temperature from 298.15 to 318.15 K reduced the selectivity, but increasing temperature further to 338.15 K somehow increased selectivity.

The H_2S/CO_2 selectivity of three ILs studied in this work is presented in Fig. 9. The effect of pressure on ILs selectivity is not pronounced for [Bmim][Ac]. But at higher pressure the selectivity increased for [Hmim][NO_3]. As for temperature, it can be seen that at higher temperature the selectivity for all three ILs was reduced. But at 298.15 K and high pressure the selectivity of H_2S over CO_2 for [Hmim][Tf_2N] was higher than that of other two ILs.

CONCLUSION

The ability of three different ILs was experimentally investigated for the absorption and separation of acid gases (CO_2 and H_2S) from a real natural gas. [Hmim][Tf_2N], [Hmim][NO_3], [Bmim][Ac] are used as a potential green solvent for the gas sweetening process. Different temperatures of 298.15 K, 318.15 K, and 338.15 K and pressure range up to 40 bar were considered for the measurements. [Bmim][Ac] showed a higher capacity of absorbing CO_2 and H_2S compared to other ILs. However, the selectivity values of CO_2/CH_4, CO_2/H_2S and H_2S/CH_4 in ILs represented the separation performance of the absorption process. [Hmim][Tf_2N] showed higher selectivity for CO_2 (or H_2S) over CH_4 in comparison with [Hmim][NO_3] and [Bmim][Ac]. It can be concluded that [Hmim][Tf_2N] can be a desirable solvent for the gas sweetening process for natural gas compared to other studied ILs. Finally, the sPC-SAFT equation of state showed a good agreement with experimental data for gas solubility of natural gas in ILs.

REFERENCES

1. M. Ramdin, Q. Chen, S. P. Balaji, J. M. Vicent-Luna, A. Torres-Knoop, D. Dubbeldam, S. Calero, T. W. de Loos and T. J. H. Vlugt, *J. Comput. Sci.*, **15**, 74 (2016).
2. S. H. Jamali, M. Ramdin, T. M. Becker, A. Torres-Knoop, D. Dubbeldam, W. Buijs and T. J. H. Vlugt, *Fluid Phase Equilib.*, **433**, 50 (2017).
3. M. Ramdin, S. P. Balaji, A. Torres-Knoop, D. Dubbeldam, T. W. de Loos and T. J. H. Vlugt, *J. Chem. Eng. Data*, **60**, 3039 (2015).
4. S. M. Hailegiorgis, S. N. Khan, N. H. H. Abdolah, M. Ayoub and A. Tesfamichael, *AIP Conf. Proc.*, **1891**, 020046 (2017).
5. Z. Feng, M. Jing-Wen, Z. Zheng, W. You-Ting and Z. Zhi-Bing, *Chem. Eng. J.*, **181-182**, 222 (2012).
6. M. Mirzaei, B. Mokhtarani, A. Badiei and A. Sharifi, *J. Chem. Thermodyn.*, **122**, 31 (2018).
7. K. Golzar, S. Amjad-Iranagh and H. Modarress, *Ind. Eng. Chem. Res.*, **53**, 7247 (2014).
8. M. B. Shiflett and A. Yokozeki, *J. Phys. Chem. B.*, **111**, 2070 (2007).
9. J. E. Bara, C. J. Gabriel, T. K. Carlisle, D. E. Camper, A. Finotello, D. L. Gin and R. D. Noble, *Chem. Eng. J.*, **147**, 43 (2009).
10. P. Scovazzo, D. Camper, J. Kieft, J. Poshusta, C. Koval and R. Noble, *Ind. Eng. Chem. Res.*, **43**, 6855 (2004).
11. S. Kumar, J. H. Cho and I. Moon, *Int. J. Greenh. Gas Control.*, **20**, 87 (2014).
12. S. K. Kailasa, J. R. Koduru, K. Vikrant, Y. F. Tsang, R. K. Singhal, C. M. Hussain and K.-H. H. Kim, *J. Mol. Liq.*, **297**, 111886 (2020).
13. N. MacDowell, N. Florin, A. Buchard, J. Hallett, A. Galindo, G. Jackson, C. S. Adjiman, C. K. Williams, N. Shah and P. Fennell, *Energy Environ. Sci.*, **3**, 1645 (2010).
14. A. Maiti, *ChemSusChem.*, **2**, 628 (2009).
15. M. Hasib-ur-Rahman, M. Siaj and F. Larachi, *Chem. Eng. Process. Process Intensif.*, **49**, 313 (2010).
16. R. E. Baltus, B. H. Culbertson, S. Dai, H. Luo and D. W. DePaoli, *J. Phys. Chem. B.*, **108**, 721 (2004).
17. D. Camper, J. E. Bara, D. L. Gin and R. D. Noble, *Ind. Eng. Chem. Res.*, **47**, 8496 (2008).
18. S. N. V. K. Aki, B. R. Mellein, E. M. Saurer and J. F. Brennecke, *J. Phys. Chem. B.*, **108**, 20355 (2004).
19. Z. Lei, C. Dai and B. Chen, *Chem. Rev.*, **114**, 1289 (2014).
20. F. Shaahmadi, B. Hashemi Shahraki and A. Farhadi, *J. Chem. Thermodyn.*, **141**, 105922 (2020).
21. S. Mortazavi-Manesh, M. A. Satyro and R. A. Marriott, *AIChE J.*, **59**, 2993 (2013).
22. Y. J. Heintz, L. Sehabiague, B. I. Morsi, K. L. Jones, D. R. Luebke and H. W. Pennline, *Energy Fuels*, **23**, 4822 (2009).
23. G. Cui, J. Wang and S. Zhang, *Chem. Soc. Rev.*, **45**, 4307 (2016).
24. B. R. Mellein, A. M. Scurto and M. B. Shiflett, *Curr. Opin. Green Sustain. Chem.*, **28**, 100425 (2021).
25. L. Y. Wang, Y. L. Xu, Z. D. Li, Y. N. Wei and J. P. Wei, *Energy Fuels*, **32**, 10 (2018).
26. A. H. Jalili, M. Mehrabi, A. T. Zoghi, M. Shokouhi and S. A. Taheri, *Fluid Phase Equilib.*, **453**, 1 (2017).
27. F. Shaahmadi, B. Hashemi Shahraki and A. Farhadi, *J. Chem. Eng. Data*, **64**(2), 584 (2019).
28. A. Grenner, G. M. Kontogeorgis, N. von Solms and M. L. Michelsen, *Fluid Phase Equilib.*, **258**, 83 (2007).
29. J. Gross and G. Sadowski, *Ind. Eng. Chem. Res.*, **40**, 1244 (2001).
30. M. Abolala and F. Varaminian, *J. Mol. Liq.*, **187**, 359 (2013).
31. J. Safarov, R. Hamidova, S. Zepik, H. Schmidt, I. Kul, A. Shahverdiyev and E. Hassel, *J. Mol. Liq.*, **187**, 137 (2013).
32. M. Iguchi, Y. Hiraga, Y. Sato, T. M. Aida, M. Watanabe and R. L. Smith, *J. Chem. Eng. Data*, **59**, 709 (2014).
33. J. M. S. S. Esperança, H. J. R. Guedes, J. N. Canongia Lopes and L. P. N. Rebelo, *J. Chem. Eng. Data*, **53**, 867 (2008).
34. R. Gomes De Azevedo, J. M. S. S. Esperança, J. Szydlowski, Z. P. Visak, P. F. Pires, H. J. R. Guedes and L. P. N. Rebelo, *J. Chem. Thermodyn.*, **37**, 888 (2005).
35. M. Kanakubo and K. R. Harris, *J. Chem. Eng. Data*, **60**, 1408 (2015).
36. K. R. Seddon, A. Stark and M.-J. Torres, *ACS Symposium Ser.*, **819**, 34 (2002).
37. Z. Khedri, M. Almasi and A. Maleki, *J. Chem. Eng. Data*, **64**, 4465 (2019).
38. Y. Hiraga, A. Kato, Y. Sato and R. L. Smith, *J. Chem. Eng. Data*, **60**, 876 (2015).
39. S. Stevanovic, A. Podgoršek, A. A. H. Pádua and M. F. Costa Gomes, *J. Phys. Chem. B.*, **116**, 14416 (2012).
40. H. F. D. Almeida, H. Passos, J. A. Lopes-da-Silva, A. M. Fernandes, M. G. Freire and J. A. P. Coutinho, *J. Chem. Eng. Data*, **57**, 3005 (2012).
41. A. H. Jalili, M. Safavi, C. Ghotbi, A. Mehdizadeh, M. Hosseini-Jenab and V. Taghikhani, *J. Phys. Chem. B.*, **116**, 2758 (2012).